

Constant-Pressure Technique for Gas Diffusivity and Solubility Measurements in Heavy Oil and Bitumen

S. Reza Etminan,* Brij B. Maini, Zhangxin Chen, and Hassan Hassanzadeh

Department of Chemical and Petroleum Engineering, University of Calgary, Calgary, Alberta, Canada

Received August 17, 2009. Revised Manuscript Received November 30, 2009

A modified pressure decay method has been designed and tested for more reliable measurements of molecular diffusion coefficients of gases into liquids. Unlike the conventional pressure decay method, the experimental setup has been designed such that the interface pressure and consequently the dissolved gas concentration at the interface are kept constant. This is accomplished by continuously injecting the required amount of gas into the gas cap from a secondary supply cell to maintain the pressure constant at the gas–liquid interface. The pressure decay is measured in the supply cell. The advantage of the new technique is that, assuming the diffusion coefficient to be constant, a simple analysis allows determination of the equilibrium concentration and diffusion coefficient.

Introduction

In view of the current high energy demand and the lack of any satisfactory alternative to petroleum and other fossil fuels for meeting this demand, it becomes apparent that the dominance of fossil fuels in the energy industry will continue for several decades. Meanwhile, the rapid decline in the known conventional oil reserves and increasing cost of finding new oil has turned the tide in favor of exploiting known heavy oil and bitumen reservoirs for our energy requirements.

Efficient recovery of heavy oil and bitumen is still very challenging and has remained an issue of ongoing research all around the world. Thermal recovery methods, which rely on heat for viscosity reduction, are generally accepted as viable, and several steam based projects have been successful, especially in Canada. However, thermal methods are energy intensive and not always cost-effective. Addition of a light hydrocarbon solvent to steam has attracted considerable attention for improving the performance of steam based recovery methods. Molecular diffusion coefficient of solvent in heavy oil is a key parameter in recovery processes involving solvent injection.

It is noteworthy that there is no well established and universally applicable technique for measuring the molecular diffusion coefficient. Unlike the measurements of viscosity or thermal conductivity, for which standardized techniques and equipment are readily available, the measurements of mass transfer characteristic are often more difficult due to difficulties in measuring point values of concentration and other issues which complicate this transport process. Phase equilibrium, effect of convective transport, and having a mixture rather than a pure fluid are some of the issues which can be enumerated. These issues make it necessary to employ several simplifying assumptions in interpreting the experiments to determine the diffusivity.

Amid the available techniques, there are methods which directly measure the concentration distribution of the dissolved species in the solution. However, these methods are relatively expensive and many of them are system-intrusive. As an alternative, several other methods have been introduced in which the diffusion coefficient is determined by measuring some other parameters that depends on gas dissolution rate. These methods in which there is no need to measure compositions directly, have been categorized by Sheikh et al.¹ as indirect methods. These parameters could be the rate of change of solution volume or movement of the gas–liquid interface,^{2,3} rate of pressure drop in a confined cell which is known as pressure decay method, rate of gas injection from the top to a cell in which the pressure and solution volume are kept constant,⁴ and some other techniques like the NMR spectra change method and CAT-scanning method,⁵ and recently dynamic pendant drop analysis.⁶

Among indirect methods, the pressure decay method has attracted more attention due to its simplicity in terms of experimental measurements. This method was first applied by Riazi⁷ and for dissolution of methane in *n*-pentane. He was recording both volume change due to dissolution and also dissolution rate from a pressure decline in the gas cap. Then Zhang et al.⁸ used the same approach but for a constant volume of solution and developed a mathematical model for it. They did not account for the movement of interface and they used constant saturation concentration of gas at the interface as the boundary condition. They tried a graphical

*To whom correspondence should be addressed. Department of Chemical and Petroleum Engineering, 2500 University Drive NW, Calgary, AB, Canada T2N 1N4. Telephone: 1-403-210-8730. Fax: 1-403-210-3973. E-mail: sretmina@ucalgary.ca.

- (1) Sheikh, H.; Pooladi-Darvish, M.; Mehrotra, A. K. *Energy Fuels* **2005**, *19*, 2041–2049.
- (2) Jamialahmadi, M.; Emadi, M.; Muller-Steinhagen, H. *J. Pet. Sci. Eng.* **2006**, *53*, 47–60.
- (3) Do, H. D.; Pinczewski, W. V. *Chem. Eng. Sci.* **1991**, *46* (5/6), 1259–1270.
- (4) Pomeroy, R. D.; Lacey, W. N.; Scudder, N. F.; Stapp, F. *Ind. Eng. Chem.* **1933**, *25* (9), 1014–1019.
- (5) Wen, Y. W.; Kantzas, A. *Energy Fuels* **2005**, *19*, 1319–1326.
- (6) Yang, C.; Gu, W. *SPE J. (Soc. Pet. Eng.)* **2006**, 48–57.
- (7) Riazi, M. R. *J. Pet. Sci. Eng.* **1996**, *14*, 235–250.
- (8) Zhang, Y. P.; Hyndman, C. L.; Maini, B. B. *J. Pet. Sci. Eng.* **2000**, *25*, 37–47.

method to find both the diffusion coefficient and the saturation concentration. However, since the saturation concentration was determined from the estimated value of equilibrium pressure (pressure of the gas cap when the oil is fully saturated with the gas and pressure in the gas cap is not declining anymore), they found the inferred diffusion coefficient to be very sensitive to the estimated equilibrium pressure. Thus, they concluded that the graphical method was not reliable, and a nonlinear regression approach was used to find the unknown parameters. More extended experimental studies were conducted on two Canadian bitumen samples and different solvent gases by Upreti and Mehrotra.^{9,10} They solved the problem numerically once a time dependent boundary condition was assigned to the interface and included both the effect of oil swelling and diffusion coefficient dependency on concentration.

Other researchers have proposed and developed different mathematical solutions by modeling the interface boundary condition differently. With dependence on how the interface boundary condition is defined, a range of simple to very complex solutions can be expected for this problem. Civan and Rasmussen^{11–14} introduced a hindered gas transfer boundary condition. They assumed existence of resistance on interface to diffusion of gas molecules and as a result added a mass transfer coefficient to model this physics. The mass transfer coefficient and diffusivity number are the two unknowns in their works. Different experimental data from other authors were applied with this mathematical model to determine the values of these two parameters. Their boundary condition at the interface is the so-called third kind or Robin type of boundary conditions which adds to the complexity of the problem. However, again like Zhang et al.,⁸ saturation concentration was bonded to concentration at the equilibrium pressure. They explained that if the mass transfer coefficient is very large, this problem acts exactly the same as Zhang et al.'s model. The diffusion coefficient was assumed to be constant, and the swelling was assumed to be negligible in their work.

Tharanivasan et al.¹⁵ compared the above-mentioned three methods with each other and called them equilibrium, quasi-equilibrium, and nonequilibrium, respectively. They concluded that depending on the dissolved gas, different boundary conditions should be applied for modeling the interface. In 2006, they¹⁶ extended their work by conducting three sets of experiments with a bitumen sample and methane, carbon dioxide, and propane. In 2005, Sheikha et al.^{1,17} modeled the physics of interface mass transfer by defining a time-dependent flux (derivative) type boundary condition which equated the rate of gas leaving the gas cap to the rate of gas diffusing into the oil body. Then they determined the diffusion coefficient using a graphical method. For the solubility term,

they introduced an instantaneous Henry's constant which relates the pressure of the gas cap to the interface gas concentration and estimated this value from Svrcek and Mehrotra's measurements.^{18,19}

Modeling the physics of the interface (when the pressure is declining) often requires complex mathematical solutions, and it is known that more simplified analysis based on assumption of constant equilibrium concentration at the interface introduces significant error in the estimation of the diffusion coefficient. The objective of this work is to develop an experimental technique to overcome some of these shortcomings of the pressure decay technique. In this study, the idea of maintaining a more reliable boundary condition at the interface was followed, which culminated in the design and construction of a constant pressure diffusion measurement setup in which the pressure in the diffusion cell is kept constant. Following the assumption of having instantaneous equilibrium at the interface, this implies a constant concentration at the interface. The constant boundary condition at the interface resulting from this modified setup allows development of a much simpler and more certain mathematical solution, which can find not only the diffusion coefficient but also the solubility or saturation concentration from the same experiment. In essence, it is a constant diffusion-cell-volume technique, in which, unlike the pressure-decay method, we are now able to measure the rate of gas dissolution while maintaining constant pressure in the gas cap so that the boundary condition at the interface does not change with time. This is accomplished by continuously injecting as much gas into the gas cap as needed to maintain constant pressure and measuring the rate of such a gas injection. Gas is provided from another cell called the "supply cell", and the rate of pressure decay is recorded in this latter cell rather than the diffusion cell. By this means, it becomes possible to accurately determine how much gas has been added to the diffusion cell or equivalently dissolved into the bitumen body.

In terms of a mathematical solution, a finite acting and infinite acting analytical solution are derived based on this boundary condition which can be fitted very well to our experimental data. Two inverse approaches have been developed, both of which determine the diffusion coefficient and solubility.

One advantage of this new experimental design is its ease of experimental validation and elimination of the need for independently determined solubility. In many other works, either the saturation concentration or Henry's constant is determined from other experimental data. It is so because finding the saturation concentration from the conventional pressure decay method is only feasible if one waits for a very long time to reach near saturation concentration. The extrapolation of the dissolution curve is often not reliable. However, in this method, saturation concentration is a parameter which is determined from our solution, and there is no need to wait for reaching near equilibrium concentration.

Another advantage of the new experimental design is that measurement of diffusion coefficients for solvent gases at pressures very close to their dew point pressure can be obtained; however, this requires a different mathematical solution that includes the effect of liquid swelling, which will be presented in a separate future publication.

(9) Upreti, S. R.; Mehrotra, A. K. *Ind. Eng. Chem. Res.* **2000**, *39*, 1080–1087.

(10) Upreti, S. R.; Mehrotra, A. K. *Can. J. Chem. Eng.* **2002**, *80*, 116–125.

(11) Civan, F.; Rasmussen, M. L. SPE Mid-Continent Operation Symposium, Oklahoma City, OK, March 2001; SPE 67319.

(12) Civan, F.; Rasmussen, M. L. SPE/DOE 13th Symposium on Improved Oil Recovery, Tulsa, OK, April 13–17, 2002; SPE 75135.

(13) Civan, F.; Rasmussen, M. L. *SPE J.* **2006**, *71*–79.

(14) Rasmussen, M. L.; Civan, F. *AIChE J.* **2009**, *55* (1), 9–23.

(15) Tharanivasan, A. K.; Yang, C.; Gu, Y. *J. Pet. Sci. Eng.* **2004**, *44* (3–4), 269–282.

(16) Tharanivasan, A. K.; Yang, C.; Gu, Y. *Energy Fuels* **2006**, *20* (6), 2509–2517.

(17) Sheikha, H.; Mehrotra, A. K.; Pooladi Darvish, M. *J. Pet. Sci. Eng.* **2006**, *53*, 189–202.

(18) Mehrotra, A. K.; Svrcek, W. Y. *J. Can. Pet. Technol.* **1982**, *21* (6), 95.

(19) Svrcek, W. Y.; Mehrotra, A. K. *J. Can. Pet. Technol.* **1982**, *21* (4), 31.

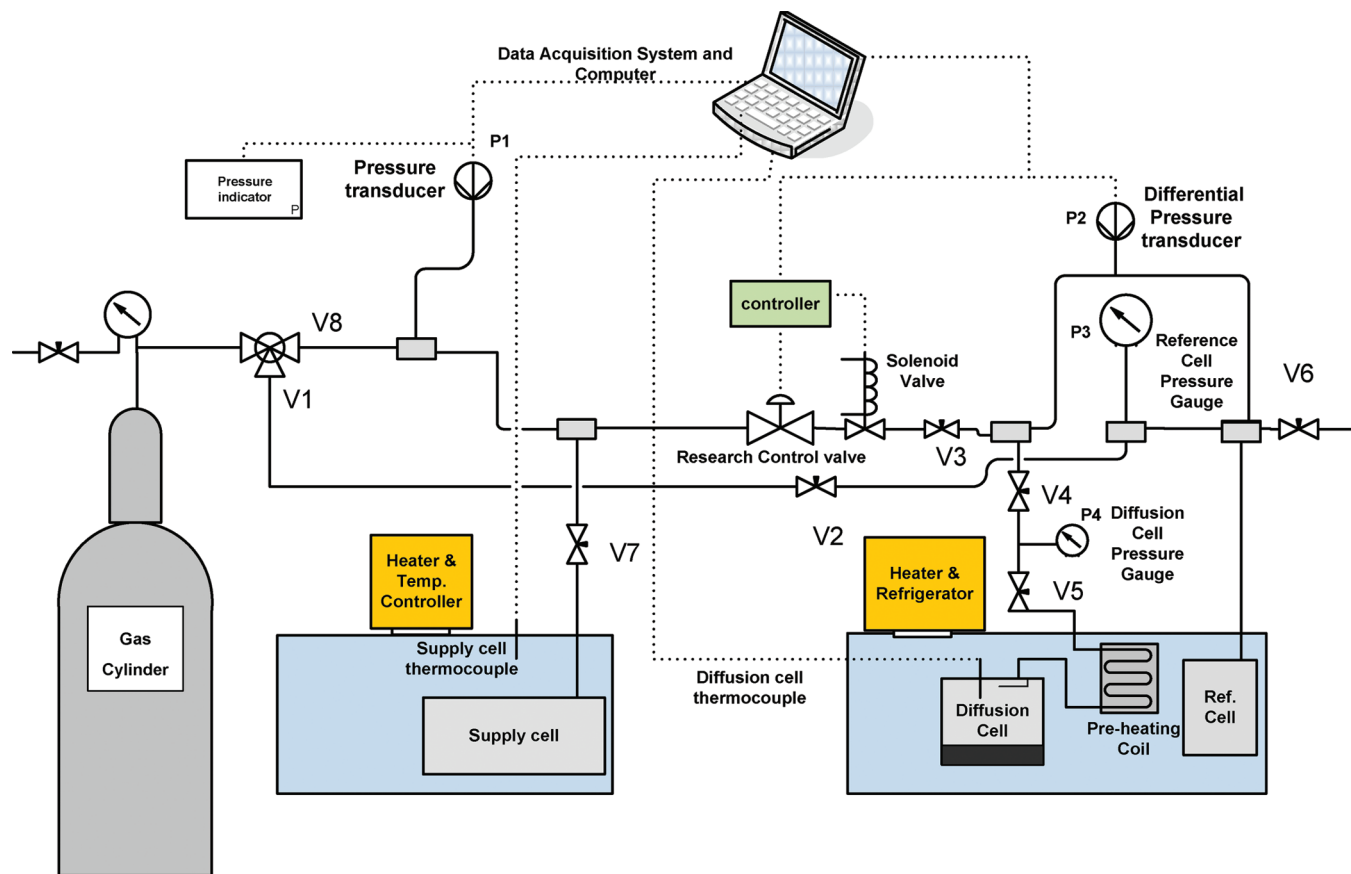


Figure 1. Experimental setup schematic.

Experimental Equipment and Measurements

Experimental Setup. A fully automated apparatus has been constructed which allows measurement of the rate of gas dissolution in the diffusion cell while keeping its pressure constant. Figure 1 shows the schematic diagram of the experimental setup. The apparatus comprises a diffusion cell, a reference cell, and a gas supply cell. The diffusion process takes place in the first cell.

The diffusion cell and the gas supply cell are connected to each other through two electronically controlled valves that operate based on the pressure difference between the diffusion cell and the reference cell. The reference cell is only used as an external constant pressure cell with which the diffusion cell pressure is compared and the difference is used as the controlling factor to let the gas in from the supply cell to the diffusion cell.

The diffusion cell is a cylindrical blind cell with an inner diameter of 6.35 cm and 5.71 cm in height and made of stainless steel. It is capped with a stainless steel lid containing two holes: one for the gas inlet and the other for a thermocouple. A small deflector is welded in front of the gas inlet hole to prevent direct discharge of gas into the liquid body. The reference cell is a small stainless steel pressure vessel. These two cells are kept in an isothermal water bath and both are connected to a Rosemount high precision differential pressure transducer. This pressure transducer can measure the pressure difference between the two cells to the accuracy of ± 0.25 kPa with span of 62.03 kPa. The connection between the supply cell and diffusion cell is through two valves: a BadgerMeter electronically actuated control valve and a miniature Asco electronic solenoid valve. It was found that the control valve does not completely shut off the gas flow even when it is fully closed. To overcome this problem, an electronic on–off solenoid valve was employed. The pressure transducer which measures the supply cell pressure is a 0.0001 %

resolution ParaScientific Digiquartz 31K-101 pressure transducer which can measure absolute pressures up to 6893 kPa (1000 psi) and with a precision of 6.89 Pa (0.001 psi). A National Instrument (NI) software module was used for pressure control. It works such that when the pressure differential, ΔP , between these two cells is positive (pressure in diffusion cell is higher), the solenoid valve and also the control valve remain closed, and when this difference becomes negative, they both open to let the gas flow into the diffusion cell. The extent to which the control valve opens depends on the magnitude of the negative pressure difference. A data acquisition system was used to display and record the data once every minute. These data comprise (1) a differential pressure between the diffusion and reference cell, (2) supply cell pressure, (3) supply bath temperature, and (4) diffusion cell temperature. Two additional pressure gauges are connected separately, one to the reference cell and the other right above the diffusion cell, which displays the pressure of these two cells.

Experimental Procedure. The first step in experiments was to make the system leak-free. The setup was pressurized and left for about 1 week to determine if there was any leakage in the system. Because of the high resolution of the pressure transducer, any small leakage was detectable from the pressure trend. In addition to this, a leak test meter was used to determine the leakage locations. Generally, leakage in these kind of systems is a serious concern, and care is required to eliminate it. After these preparatory steps, the following procedure was followed in each experiment.

(i) First, the empty diffusion cell is weighed, and the specified amount of liquid is poured gradually to reach to the desired liquid weight. In case the liquid is viscous, like bitumen, some time is allowed to let any trapped air escape. (ii) The gas line and thermocouple at the top of the cell are then connected, and the diffusion cell is placed beside the reference cell in a temperature

Table 1. Summary of Conducted Experiments

experiment no.	solute	solvent	diffusion cell gauge P (kPa)	diffusion cell temperature ($^{\circ}\text{C}$)	supply cell initial absolute P (kPa)	supply cell final absolute P (kPa)	run duration (h)	liquid height (cm)	to be compared with
1	CH_4	dodecane	3460.2	65	3818.088	3767.193	235.2	3.00	Jamialahmadi et al. ^a
2	CH_4	dodecane	3446.4	45	3754.578	3596.429	360.6	3.00	
3	CO_2	athabasca bitumen	3239.6	75	3408.066	3397.610	172.2	1.05	Upreti et al. ^b
4	CO_2	athabasca bitumen	3804.8	50	3998.882	3984.656	278.7	1.00	Sheikha et al. ^c Rasmussen et al. ^d

^a Refer to ref 2. ^b Refer to refs 9 and 10. ^c Refer to ref 1. ^d Refer to ref 14.

Table 2. Comparison of Experiments 1 and 2 with the Results of Jamialahmadi et al.^a, Diffusion Coefficient Comparison

	this work	work of Jamialahmadi et al. ^a
method used	modified pressure decay method	interface movement tracking method
specifications	constant pressure in diffusion cell	constant pressure in diffusion cell
BC at interface	Dirichlet BC nonhomogenous constant value	Dirichlet BC nonhomogenous constant value
diffusivity, cm^2/s	Experiment 1: Methane and Dodecane at $P = 3460$ kPa and $T = 65$ $^{\circ}\text{C}$ 4.86×10^{-5}	10.6×10^{-5}
diffusivity, cm^2/s	Experiment 2: Methane & Dodecane at $P = 3446.4$ kPa and $T = 45$ $^{\circ}\text{C}$ 4.32×10^{-5}	9.0×10^{-5}

^a Refer to ref 2.

controlled water bath. As it can be seen in Figure 1, a preheating (precooling) coil is provided to heat or cool the gas coming into the diffusion cell during the measurements. Furthermore, all the lines are covered by a layer of wool and aluminum foil to minimize heat exchange with the room air. (iii) Air in the gas cap of the diffusion cell is extracted using a vacuum pump by alternating the connection of the diffusion cell to the vacuum line and the gas supply line. Only a light vacuum is used, and it is done only for a short time to avoid evaporation of the test oils. The aim is to remove the air from the gas cap and replace it with the test gas. (iv) After confirmation that the reference and diffusion cells are at the same constant temperature, the reference cell pressurization starts. Gas starts filling the reference cell to the reference pressure that is intended to be used as our diffusion pressure. The pressure gauge, P3, is used to measure the pressure inside the reference cell. (v) The supply cell is then pressurized. The supply cell temperature is controlled using a separate controlled-temperature water bath. The temperature of this cell can be any arbitrary temperature, but care has to be taken not to have gas condensation due to temperature and pressure change once it flows toward the diffusion cell. It is the supply cell that is used to pressurize the diffusion cell. So, it needs to be pressurized such that it provides enough gas for both gas cap pressurization and gas dissolution. By this means, the amount of gas that is used to pressurize the gas cap can be measured to determine how much gas has been dissolved during the pressurization period. This was estimated and was determined to be totally negligible. Once the supply cell is pressurized, some time is given for the gas to reach a stabilized pressure at the bath temperature. (vi) The final step is pressurization of the diffusion cell gas cap and start of the experiment. By opening valve V3 and operating the control valve manually, gas is directed to pressurize the diffusion cell. This is continued until the gas cap reaches the same pressure as the reference cell, and then both valves are shut off and the system switched to automatic control immediately.

The pressure difference between the two cells (P2) is measured, and the frequency and amplitude of the pressure change in the diffusion cell is recorded every minute. It was noted that when the dissolution rates are high, the two intelligent valves open and close more frequently and the pressure in the diffusion cell is kept always close to the desired pressure. Once the dissolution rate goes down, this frequency becomes lower and

the pressure fluctuations get somewhat larger. The pressure change values and the relative errors due to this fluctuation in each experiment are described in Table 7.

Experiments and Materials. In this paper, four experiments are described which were at conditions at which diffusivity coefficients have been reported by other researchers. These experiments were used as validation of this technique. Experimental conditions are summarized in Table 1.

In experiments 1 and 2, a binary system of methane and dodecane was used at operating conditions of about 3450 kPa and 65 and 45 $^{\circ}\text{C}$, respectively. Our results have been compared with the results of Jamialahmadi et al.² who measured binary diffusion coefficients of these two components by using the interface tracking method. A liquid column height of 3 cm dodecane was initially located in the diffusion cell in both experiments, and the tests were run for 10 and 15 days, respectively. The supply cell temperatures of experiments 1 and 2 were 40 ± 0.10 and 40 ± 0.05 $^{\circ}\text{C}$, and the diffusion cell temperatures were 65 ± 0.15 and 45 ± 0.10 $^{\circ}\text{C}$, respectively. In experiments 3 and 4, carbon dioxide and Athabasca bitumen were used. These two experiments were designed to be directly comparable to the experiments of Upreti et al.⁹ and to the results of the evaluations of Upreti's experiments by Sheikha et al.¹ and Rasmussen et al.¹⁴ The temperatures in the supply cell in these two experiments were 30 ± 0.10 and 35 ± 0.05 $^{\circ}\text{C}$, respectively. The diffusion cell temperatures were 75 ± 0.50 and 50 ± 0.10 $^{\circ}\text{C}$. The diffusion cell's temperature variation in the third experiment was more significant than the other three experiments. Since an open heating bath was being used in our experiment, due to high rate of bath liquid evaporation, the temperature control at higher temperatures was more difficult. Figures 6 and 8 present the gas dissolution data in these two experiments. The big dissolution jump around 55th hour was due to a malfunction in the pressure control. However, as it is shown later in this paper, this outlier does not influence our predicted results significantly. The supply cell initial and final pressures are also listed in Table 1.

The gases used for our experiments were all provided by Praxair. The purity of methane and carbon dioxide were 99.97 and 99.9 wt %, respectively. The 98.5% purity normal dodecane was purchased from FisherScientific. Its molecular weight, density, and boiling point were 170.34 g/g mol, 753 kg/m³, and 216.2 $^{\circ}\text{C}$, respectively.

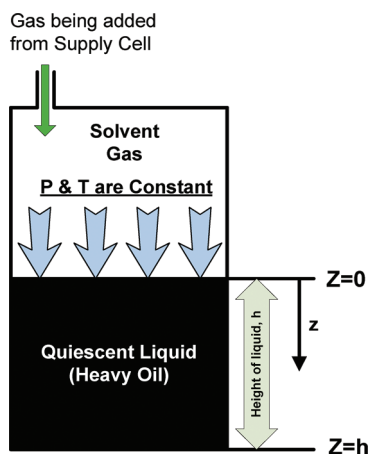


Figure 2. Schematic of diffusion cell and our model coordinates.

The Athabasca bitumen was the same coker feed sample, obtained from Syncrude Canada Ltd. that Badamchizadeh et al.²⁰ used in their studies. The densities of bitumen at the operating conditions of experiments 3 and 4 were 972.5 and 988.3 kg/m³, respectively. The asphaltene content of this oil is 16.1 wt %, and its molecular weight is 552 g/g mol. The viscosity of this bitumen is about 100000 mPa.s at 50 °C, and 10000 mPa.s at 80 °C.

Theory and Mathematical Model

Forward Problem. There are three important parameters that govern the mass transfer during dissolution of a gas into a nonvolatile liquid in a binary system. These are (1) equilibrium concentration of gas in the liquid, (2) molecular diffusivity, and (3) mass transfer coefficient. The last one is important only when there is significant interfacial resistance to mass transfer. As Sheikha et al.¹ have also explained, the equilibrium concentration or gas solubility is the maximum concentration of gas that will dissolve in the oil at the prevailing thermodynamic conditions and in absence of interfacial resistance, the liquid at the interface attains this concentration instantaneously. The second parameter is the diffusion coefficient which controls the rate of mass transfer within the liquid,¹⁷ and finally the mass transfer coefficient is defined as a proportionality constant that relates the mass flux to the difference between the equilibrium liquid-phase concentration and the current concentration on the liquid side of the interface.²¹

Figure 2 depicts the schematic of the diffusion cell. The quiescent liquid column is at the bottom of the cell, and the cell pressure is kept constant during the experiment.

The gas–liquid interface is located at $z = 0$, and the cell's bottom is located at $z = h$. The diffusion of gas from the gas cap into the liquid column can be modeled as a one-dimensional unsteady diffusion problem using Fick's second law:

$$\frac{\partial^2 C_g}{\partial z^2} = \frac{1}{D} \frac{\partial C_g}{\partial t} \quad (1)$$

where C_g is the concentration of gas in the quiescent liquid column, z is the distance from the interface, t is time, and D is the diffusion coefficient. In the above equation, D is assumed

to be a constant average diffusion coefficient. This simplifying assumption is valid when the solubility of gas into the liquid is not high under the test conditions. Several other assumptions are implicit in using the above equation to model the process: (1) diffusion happens at isothermal conditions; (2) there is no chemical reaction between the solvent gas and the quiescent liquid; (3) liquid is nonvolatile and there is only a one-way transfer from gas to the liquid; (4) swelling of the liquid column due to the dissolution of gas is negligible; (5) there is no mass transfer resistance at the interface and a thermodynamic equilibrium prevails instantly at the interface; and (6) the density of solution is lower than pure liquid, and thus there will not be any natural convection. Consequently, no convective mixing happens in the liquid column.

For this study, gas and liquid samples were used which closely meet all the above conditions. Nevertheless, errors due to some of these simplifying assumptions have been estimated and reported at the Error Analysis Section.

Knowing that liquid sample is initially free of solvent gas, the initial condition is

$$C_g(z, t = 0) = 0 \quad (2)$$

Thermodynamically, once the pressure and temperature are kept constant in the gas cap (there is no pressure gradient inside the gas cap since it is a small open medium), assuming an instant equilibrium at the interface is acceptable. Therefore, the concentration of gas in liquid at the interface is the saturation concentration or ultimate solubility of gas in the liquid. In this case, the interface boundary condition becomes a nonhomogenous constant-value Dirichlet type boundary condition as

$$C_g(z = 0, t) = C_g^* \quad (3)$$

where C_g^* is the saturation concentration. It is evident that solution of the partial differential equation, analytically or numerically, using a single-value boundary condition at the interface is much easier compared to solving it with a time dependent boundary condition at the interface or with the added uncertainty of assigning a late time equilibrium concentration to the interface from the beginning, as was done by Zhang et al.⁸ and later by Tharanivasan et al.¹⁶

The second boundary condition can be taken as either one of two possible cases. First, a semi-infinite domain can be used, which physically is like having a bottomless diffusion cell. With this boundary condition, the solution would be only correct as long as the gas concentration has not touched the cell's bottom. The second approach is to use a no-flow boundary at $z = h$. We have solved the problem with both of these boundary conditions.

$$\text{for the semi-infinite domain : } C_g(z \rightarrow \infty, t) = 0 \quad (4)$$

$$\text{finite domain : } \frac{\partial C_g}{\partial z}(z = h, t) = 0 \quad (5)$$

A simple material balance on the gas and liquid leads to an equation which describes the dissolution process. Since the pressure in the gas cap remains constant, this becomes a material balance between the gas that leaves the supply cell (to be added to diffusion cell) and the gas that diffuses into the liquid body. Thus, knowing the initial pressure of supply cell and the subsequent lower pressure gives us the amount of gas transfer from the supply cell to the diffusion cell. The

(20) Badamchi-Zadeh, A.; Yarranton, H. W.; Svrcek, W. Y.; Maini, B. B. *J. Can. Pet. Technol.* **2009**, 48 (1), 54–55.

(21) Asano, K. *Mass Transfer from Fundamental to Modern Industrial Applications*; Wiley-VCH: Weinheim, Germany, 2006; pp 21–22.

mass balance for the supply cell can be written as

$$m_{g-tr}(t) = m_{g-ini} - m_{g-r}(t) \\ = \frac{V_{SC} M_w}{R} \left(\frac{P_{ini}}{Z_{ini} T_{ini}} - \frac{P(t)}{Z(t) T(t)} \right)_{SC} \quad (6)$$

where $m_{g-tr}(t)$ is the mass of gas transferred from supply cell to diffusion cell (gram) which is determined by subtraction of $m_{g-r}(t)$, the remained gas in the supply cell from m_{g-ini} , which is the initial gas in the supply cell. P_{ini} is the supply cell initial pressure (in kilopascals); V_{SC} is the supply cell volume (in cubic centimeters); Z_{ini} is the gas compressibility factor at initial pressure; $P(t)$ is the supply cell pressure at time t (in kilopascals); $Z(t)$ is the gas compressibility factor at time t ($P(t) < P_{ini}$); R is the gas constant, 8314.477 kPa cm³/g mol K; $T(t)$ is the supply cell temperature at time t (in Kelvin); T_{ini} is the initial supply cell temperature (in Kelvin); M_w is the molecular weight (in gram/gram mole).

Unlike some other works in this area,^{1,8,17} the gas compressibility was not assumed to be constant and Peng–Robinson (PR) equation of state²² was applied to predict the gas compressibility factor at each time step.

The mass rate of gas diffusing into the liquid body could be modeled by Fick's first law as

$$\frac{dm_{gD}}{dt} = -DA \left(\frac{\partial C_g}{\partial z} \right)_{z=0} \quad (7)$$

where D is the intrinsic diffusivity of the gas into the liquid (in square centimeters per second); A is the cross-sectional area normal to the direction of diffusion (in square centimeters per second); and m_{gD} is the cumulative mass of gas transferred to the liquid through the interface (in grams).

If the pressure in the diffusion cell is kept always constant, the rate of gas dissolution dm_{gD}/dt in the oil body should be equal to the rate of gas addition to the gas cap (or the rate of gas withdrawal from the supply cell), which is the derivative of eq 6. In this case, these two are equal to each other at the gas–liquid interface. Since eq 6 is in the form of cumulative mass withdrawal from the supply cell or dissolved gas, an integrated form of eq 7 is used as eq 8.

$$m_{gD}(t) = \int_{t=0}^t \frac{\partial m_{gD}}{\partial t} dt = \int_{t=0}^t -DA \frac{\partial C_g}{\partial z} \Big|_{z=0} dt \quad (8)$$

For the right-hand side of eq 8, the forward solution of $C_g(z, t)$ is required. The forward solutions of the main problem for finite acting and infinite acting conditions have been determined using the Laplace transform method. The analytical solution for the finite acting and infinite acting boundary conditions are given in the following.

Finite Acting Behavior. The finite acting solution of the problem is given by²³

$$C_g(z, t) = C_g^* \left[1 - \frac{4}{\pi} \sum_{n=1}^{\infty} \frac{1}{2n-1} \sin \left(\frac{(2n-1)\pi z}{2h} \right) \exp \left(\frac{-(2n-1)^2 \pi^2 D}{4h^2} t \right) \right] \quad (9)$$

With the use of the above forward solution, differentiating it first with respect to z and finding its value at $z = 0$ and subsequently integrating it over the experimental time, leads to eq 10, which is the solution of the right-hand side of eq 8.

$$m_{gD}(t) = \frac{8AC_g^*h}{\pi^2} \sum_{n=1}^{\infty} \frac{1}{(2n-1)^2} \left[1 - \exp \left(\frac{-(2n-1)^2 \pi^2 D}{4h^2} t \right) \right] \quad (10)$$

The equality of eqs 6 and 10 ties our experimental measurements to the prediction of the two unknowns in eq 10, which are the diffusion coefficient, D , and saturation concentration term, C_g^* . This solution is valid for the entire time of the experiment. An inverse problem approach would be used to determine the values of these two unknowns.

Infinite Acting Solution. The forward infinite acting solution is given by²³

$$C_g(z, t) = C_g^* \operatorname{erfc} \left(\frac{z}{2\sqrt{Dt}} \right) \quad (11)$$

The infinite acting and finite acting solutions are identical as long as the diffusion has not penetrated to $z = h$. The use of the above solution and finding the cumulative values based on eq 8, leads to

$$m_{gD} = 2AC_g^* \sqrt{\frac{Dt}{\pi}} \quad (12)$$

Again with the right-hand side of this equation equal to eq 6, the diffusion coefficient and saturation concentration can be obtained which appear here as a composite term. This solution can be used only to determine the combined term $C_g^*(D)^{1/2}$, which simplifies the initial guess of the values of C_g^* and D in the minimization section. The finite acting solution has been used in both of our proposed inverse solutions for estimation of these two unknowns.

Inverse Problem and Parameter Estimation. As Aster et al.²⁴ have explained in their book, in many cases we want to determine a finite number of parameters to define a model. These parameters may define a physical entity directly or may be coefficients or other constants in a functional relationship that describes a physical process. Such problems are called discrete inverse problems or parameter estimation problems. Our problem here is a parameter estimation problem since, as it was explained earlier, the values of two unknowns in eq 10 are required.

The two methods which are used for evaluation of these two unknowns consist of a minimization technique and a graphical method. The first one iterates on both unknowns and finds the best solution based on an appropriate initial guess. It is relatively fast and uses all the data points recorded from the experiment. The second method is a graphical approach which will be described later.

Estimation by Error Minimization. In this section, a nonlinear least-squares method is described to minimize the error between the experimental and computed values. This leads to a system of nonlinear equations which were solved by Newton's method²⁵ that converges after 2 to 3 iterations

(22) Danesh, A. *PVT and Phase Behaviour of Petroleum Reservoir Fluids*; Elsevier: Amsterdam, The Netherlands, 2003; pp 140–141.

(23) Crank, J. *The Mathematics of Diffusion*, 2nd edition; Clarendon Press: Oxford, U.K., 1975; p 47.

(24) Aster, R. C.; Borchers, B.; Thurber, C. *Parameter Estimation and Inverse Problem*; Elsevier Academic Press: Amsterdam, The Netherlands, 2004; pp 2–3.

(25) Kelly, C. T. *Solving Nonlinear Equations with Newton's Method*; Society for Industrial and Applied Mathematics: Philadelphia, PA, 2003; pp 1–3.

in case the given initial guess is close to real values. The time dependent error term is defined as below:

$$e_i = (m_{g-tr}(t_i) - m_{gD}(t_i)) \quad (13)$$

On the basis of the least-squares method, the objective function S is defined as

$$S = \sum_{i=1}^k e_i^2 = \sum_{i=1}^k \left(\frac{V_{SC} M_w}{RT(t_i)} \left(\frac{P_{ini}}{Z_{ini}} - \frac{P(t_i)}{Z(t_i)} \right) - \frac{8AC_g^*}{\pi^2} \sum_{n=1}^{\infty} \frac{1}{(2n-1)^2} \left[1 - \exp\left(\frac{-(2n-1)^2 \pi^2 D}{4h^2} t_i \right) \right] \right)^2 \quad (14)$$

where k is the number of experimental measurements. For S to be a minimum based on the D and C_g^* values, the derivative of S with respect to these two parameters should be zero.

$$f = \frac{\partial S}{\partial C_g^*} = 0 \quad (15)$$

$$g = \frac{\partial S}{\partial D} = 0 \quad (16)$$

Each of the above derivatives were determined analytically, and then Newton's method^{25,26} was applied to reach to new D and C_g^* values. The general form of the equations for our problem is given by

$$\tilde{f}'(x_i) \Delta \tilde{x}_{i+1} = -\tilde{f}(x_i) \quad (17)$$

In this equation, $\tilde{f}'(x_i)$ is the Jacobian matrix which includes the partial derivative of f and g with respect to x_i , and $\tilde{f}(x_i)$ is a vector containing the values of f and g at x_i values, and $\Delta \tilde{x}_{i+1}$ is the difference between the new and old values of x_i . On the basis of this, one can write

$$J(D_p, (C_g^*)_p) \begin{pmatrix} \Delta D_{p+1} \\ (\Delta C_g^*)_{p+1} \end{pmatrix} = - \begin{pmatrix} f_p \\ g_p \end{pmatrix} \quad (18)$$

$$J(D, C_g^*) = \begin{bmatrix} \frac{\partial f}{\partial D} & \frac{\partial f}{\partial C_g^*} \\ \frac{\partial g}{\partial D} & \frac{\partial g}{\partial C_g^*} \end{bmatrix} = \begin{bmatrix} \frac{\partial^2 S}{\partial D \partial C_g^*} & \frac{\partial^2 S}{\partial C_g^* \partial D} \\ \frac{\partial^2 S}{\partial D^2} & \frac{\partial^2 S}{\partial C_g^{*2} \partial D} \end{bmatrix} \quad (19)$$

In eq 18, subscript p is the iteration number. Once all the values are inserted into the above equation, the new D and C_g^* values are determined. A strategy will be explained later to show how very good initial guesses can be selected for these two values. By this means, we determine two unknowns from the same experimental data and this would be really cost-effective because usually separate experiments are required for solubility measurements. In the next sections, we will use this minimization method to estimate D and C_g^* using our experimental measurements and comparing our predictions with the results available in the literature.

Graphical Method. A graphical method was also developed which can determine the values of the diffusion coefficient and the saturation concentration. As Sheikh et al.¹

have stated in their work, such methods are widely used in petroleum engineering for the determination of oil and gas reservoirs' permeability.

The infinite series in eq 10 converges very fast and can be approximated by only its first eigenvalue if t becomes quite large. In that case, eq 10 simplifies to

$$m_{gD}(t) = \frac{8AhC_g^*}{\pi^2} \left[1 - \exp\left(\frac{-\pi^2 D}{4h^2} t \right) \right] \quad (20)$$

For finding our unknowns with the graphical method, the natural logarithm of the m_g derivative with respect to time is evaluated as below:

$$\ln\left(\frac{dm_{gD}(t)}{dt}\right) = \ln\left(\frac{2AC_g^* D}{h}\right) - \left(\frac{\pi^2 D}{4h^2}\right)t \quad (21)$$

Equation 21 shows that a plot of $\ln(dm_g/dt)$ versus time results in a straight line with a slope of $-\pi^2 D/4h^2$ and an intercept of $\ln(2AC_g^* D/h)$. The slope of the fitted straight line can be used to calculate diffusivity and its intercept allows finding ultimate solubility amount. Practically, real data has always some scatter, thus there are fluctuations in the numerically determined derivative of experimental data. Therefore, these measured data should be smoothened first before finding the derivative value of m_g .

It is important to know what section of experimental data should be used to evaluate these two unknowns. It was found that $\ln(dm_g/dt)$ versus t can be divided into three regions in terms of the shape of the obtained graph out of which the middle region provides us the most useful information and the first and last sections are not that useful for the graphical technique. Details of these regions have been elaborated in the next section. The useful information is along a straight line, and then generally after reaching about 80% of the equilibrium dissolution amount, a trend of scattered data appears which does not allow meaningful interpretation. In Table 5, the starting time of these scattered data region are reported.

Results and Discussion

As shown in Table 1, the experimental data of four experiments have been used to check the validity of this experimental setup and our mathematical models. On the basis of the two solutions described above, the diffusion coefficients and solubility of each experiment have been determined and the results and estimated errors have been reported. As mentioned earlier, the gas compressibility factor was not assumed constant and its values were calculated at the corresponding pressures. The only major assumption which needs to be addressed here is neglecting the liquid swelling factor. At the end of this section, a sensitivity analysis shows the range of errors introduced into our calculations due to this assumption and whether or not this assumption is reasonable and adequate.

Estimation of Diffusivity and Ultimate Solubility Using the Minimization Technique. An initial guess for saturation concentration and diffusivity is required. The final values are determined by minimization of the error between the experimental and computed values. How these two values can be guessed properly is discussed here. For finding these initial guesses, one could use reported values from similar systems. The other alternative, which we have used is that if we plot the experimental data in a graph of the cumulative

(26) Hoffman, J. D. *Numerical Methods for Engineers and Scientists*; Marcel Dekkar: New York, 2001; pp 169–172.

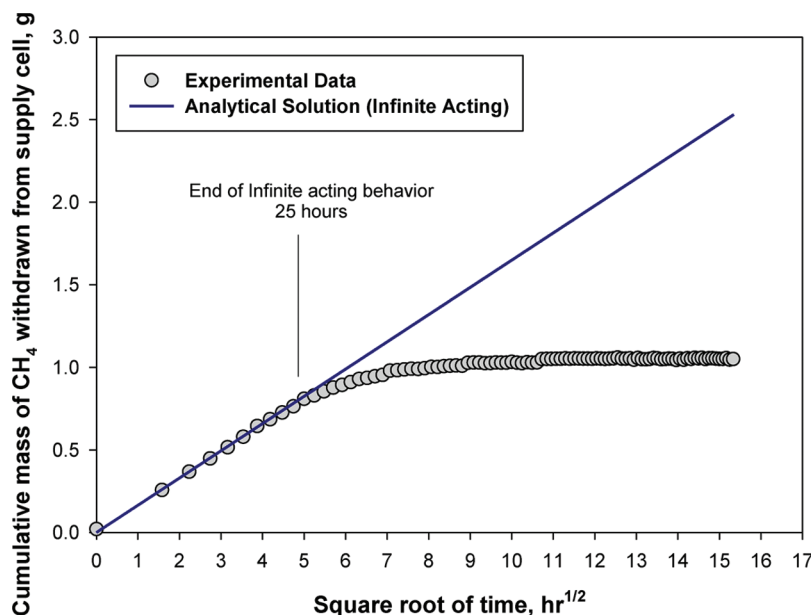


Figure 3. Cumulative mass of CH₄ withdrawn from the supply cell vs the infinite acting analytical-model plot for $D = 4.86 \times 10^{-5} \text{ cm}^2/\text{s}$ and $C_g^* = 0.01103 \text{ g/cm}^3$; system of CH₄ and dodecane at $P = 3460.2 \text{ kPa}$ and $T = 65^\circ\text{C}$.

Table 3. Comparison of Experiments 1 and 2 Solubility Results

solubility, g/cm ³	this work	Jamialahmadi et al. ^c work	CMG Winprop prediction 1	CMG Winprop prediction 2
Experiment 1: Methane and Dodecane at $P = 3460 \text{ kPa}$ and $T = 65^\circ\text{C}$				
Experiment 2: Methane and Dodecane at $P = 3446.4 \text{ kPa}$ and $T = 45^\circ\text{C}$				
experiment 1	0.01103	0.00946	0.01100	0.01031
experiment 2	0.01168	0.01211	0.01186	0.01116
solubility difference between experiments 1 and 2	0.65×10^{-3}	2.65×10^{-3}	0.86×10^{-3}	0.84×10^{-3}
^c Refer to ref 2.				

Table 4. Comparison of Experiments 3 and 4 with Three Other Results, Solubility and Diffusivity Comparison

	this work	Upreti et al. ^a	Sheikha et al. ^b	Rasmussen et al. ^c
method: pressure decay	modified	conventional	conventional	conventional
specifications of interface	constant pressure	pressure decays	pressure decays	pressure decays
BC at interface	Dirichlet	Dirichlet	Neumann	Robin
	nonhomogenous	nonhomogenous	changes with time	nonhomogenous
	constant value	changes with time		constant
Experiment 3: CO ₂ and Athabasca Bitumen at $P = 3239.6 \text{ kPa}$ and $T = 75^\circ\text{C}$				
diffusivity, cm ² /s	5.00×10^{-6}	3.74×10^{-6}	5.08×10^{-6}	5.03×10^{-6}
solubility, g/cm ³	0.03414	0.03288 ^d		0.03430
Experiment 4: CO ₂ and Athabasca Bitumen at $P = 3804.8 \text{ kPa}$ and $T = 50^\circ\text{C}$				
diffusivity, cm ² /s	3.60×10^{-6}	2.34×10^{-6}		
solubility, g/cm ³	0.03934	0.03818 ^d		

^a Refer to refs 9 and 10. ^b Refer to ref 1, Graphical method I. ^c Refer to ref 14. ^d These numbers have been calculated from Upreti's Ph.D. thesis³⁰ by an extrapolation of dissolution in infinity.

mass of solute dissolved versus square-root of time, we would be able to find reasonable initial estimates for these two unknowns. As it is shown in Figure 3, during the infinite acting period, the amount of gas dissolution plotted against the square root of time fits a straight line. The slope of this straight line helps us find the best estimates for the product of solubility and the square root of diffusivity (see eq 12). At the same time, determination of a guess for the solubility is not difficult from the late time data of the amount of solute dissolved. Thus, a combination of these two approaches provides reasonable initial guesses for diffusivity and saturation concentration.

In the following, the finite acting solutions of all four experiments are discussed. The solubility and diffusivity values of these experiments are presented in Tables 2, 3 and 4.

Experiments 1 and 2. Operating conditions and gas–liquid components in experiments 1 and 2 were selected from the work of Jamialahmadi et al.,² and we compare our results with their reported values. Results of these two experiments are reported in Tables 2 and 3. Before any comparison between our determined values and their results, it should be noted that all the numerical values of their experimental data were obtained by digitizing the measurements reported in the form of plots. Therefore, the values reported here as

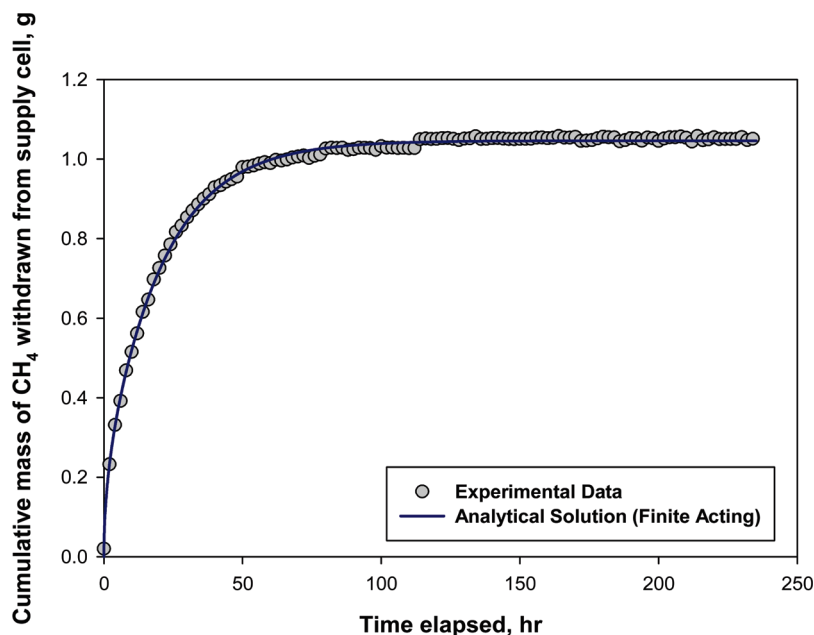


Figure 4. Cumulative mass of CH₄ withdrawn from the supply cell vs finite acting analytical-model plot for $D = 4.86 \times 10^{-5} \text{ cm}^2/\text{s}$ and $C_g^* = 0.01103 \text{ g/cm}^3$; system of CH₄ and dodecane at $P = 3460.2 \text{ kPa}$ and $T = 65^\circ\text{C}$.

Jamialahmadi et al.'s diffusivity and saturation concentration might involve some digitizing errors. With this kept in mind, as it is evident from Table 2, our diffusion coefficient values are about half of theirs. As shown in Table 3, the saturation concentration in our experiment 1 is somewhat larger than theirs and for experiment 2, it is closer. Before discussion of these differences, it is important to show that the trend of our evaluated diffusion coefficient and solubility are reasonable. Results show that as it is expected, predicted diffusivity increases with temperature while the solubility decreases. A possible reason for why these results are different from those reported by Jamialahmadi et al.² is that they have used an interface movement tracking method which is based on the swelling of the liquid as a result of dissolution. At 3450 kPa, the expected ultimate interface movement (based on gas solubility) is only about 1.5 mm, which could make the tracking of the interface more difficult.

The measurements of diffusivity and saturation concentration are reasonably close in these two works. However, there is no obvious way to say which set is more reliable. We can only compare the change of the diffusion coefficient and saturation concentration with the 20 °C temperature change (from 45 to 65 °C) with predictions from correlations.

To check whether the change in diffusivity is consistent with the temperature change in experiments 1 and 2, the Wilke-Chang²⁷ equation for prediction of diffusivity in dilute binary liquids was used which relates the diffusivity to temperature by

$$D_{AB} = 7.4 \times 10^{-8} \frac{\sqrt{\varphi_B M_{WB}} T}{\mu \tilde{V}_A^{0.6}} \quad (22)$$

where \tilde{V}_A is the molar volume of the solute A in cubic centimeters/(gram mole) as liquid at its normal boiling point, μ is the viscosity of the solution in centipoises, φ_B is an association parameter for the solvent, and T is absolute temperature in

Kelvin. It should be stressed that we are not using this equation to predict diffusivity but only the change of diffusivity with temperature. The consistency of the predicted diffusivities at the two test temperatures of 45 and 65 °C is evaluated using eq 22. From the ratio of the absolute temperatures, the Wilke-Chang²⁷ relation gives a diffusivity ratio of $D_{45}/D_{65} \equiv T_{45}/T_{65} \approx 0.94$. Our analysis gives $D_{45}/D_{65} \approx 0.89$, and Jamialahmadi et al.²'s approach results in a diffusivity ratio of 0.85.

In Table 3, the predicted ultimate solubility values have been compared with those extracted from Jamialahmadi et al.² In the third and forth columns, predictions of saturation concentration from a thermodynamic software package, Computer Modeling Group (CMG) Winprop 2008 module, is presented. Winprop is CMG's equations of state multiphase equilibrium and properties calculation program.²⁸ With a two phase flash calculation run, it is possible to find the equilibrium solubility of methane in dodecane at selected pressure and temperature. However, the results vary somewhat depending on the overall composition of the binary mixture. Physical and critical properties of methane are available in the component library of Winprop. For dodecane, the normal boiling point, specific gravity, and molecular weight were applied to estimate the other properties for use with the Peng–Robinson EOS. By using a thermodynamic software package for solubility predictions, we are not attempting to validate either of the values. We are only interested in checking the consistency of saturation concentration "variability" in going from 65 to 45 °C. The last row of Table 3 shows the incremental difference in solubility as a result of temperature reduction. It is evident that Jamialahmadi et al.'s difference is about 4 times larger than ours, but our difference is close to any of two predictions from Winprop.

Figures 4 and 5 depict a comparison of analytical solutions using predicted parameters and experimental data for experiments 1 and 2, respectively. In Figure 5, the deviation from analytical model for elapsed time after about 320 h is

(27) Bird, R. B.; Stewart, W. E.; Lightfoot, E. N. *Transport Phenomena*, 2nd ed.; John Wiley & Sons, Inc.: New York, 2002; p 530.

(28) Computer Modeling Group (CMG). *Winprop, Phase Property Program User's Guide*, 2008.

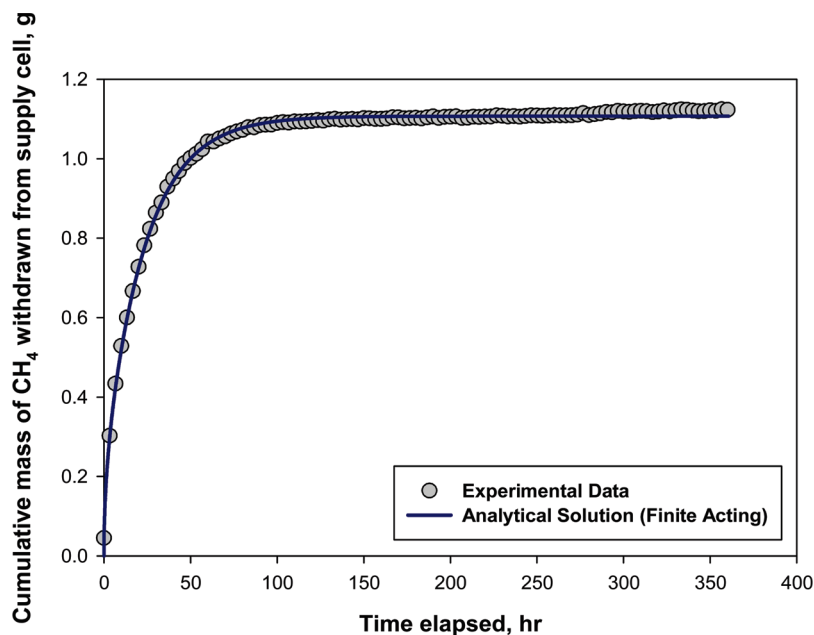


Figure 5. Cumulative mass of CH₄ withdrawn from the supply cell vs finite acting analytical-model plot for $D = 4.32 \times 10^{-5} \text{ cm}^2/\text{s}$ and $C_g^* = 0.01168 \text{ g/cm}^3$; system of CH₄ and dodecane at $P = 3446.4 \text{ kPa}$ and $T = 45^\circ\text{C}$.

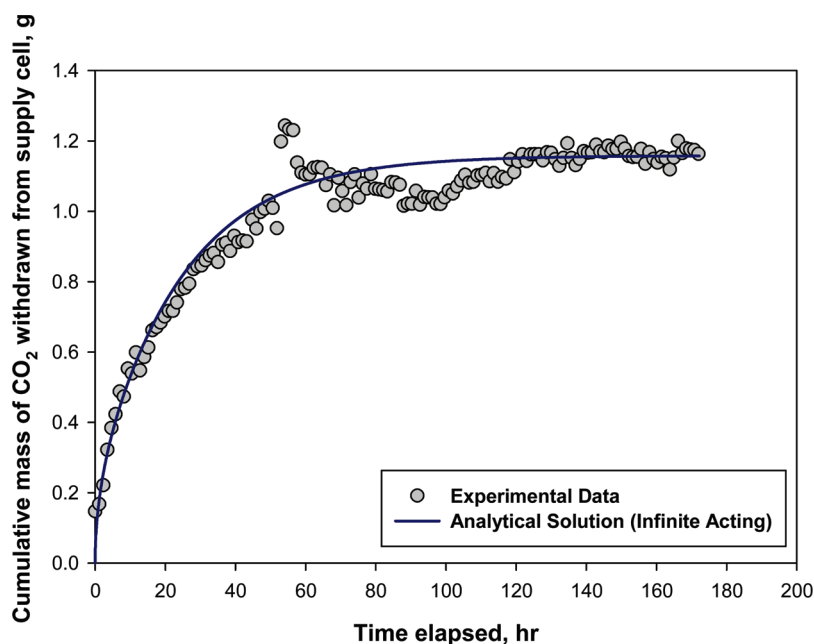


Figure 6. Cumulative mass of CO₂ withdrawn from the supply cell vs the finite acting analytical-model plot for $D = 5.00 \times 10^{-6} \text{ cm}^2/\text{s}$ and $C_g^* = 0.03414 \text{ g/cm}^3$; system of CO₂ and Athabasca bitumen at $P = 3239.6 \text{ kPa}$ and $T = 75^\circ\text{C}$.

related to a drop in the supply cell heating bath liquid level which affected the supply cell temperature.

Experiments 3 and 4. Experiments 3 and 4 were designed to be compared with the results of Upreti et al.^{9,10}, Sheikha et al.¹, and Rasmussen et al.¹⁴ for diffusivity and solubility values. The mathematical models in these three works are quite different from our work. The boundary condition types at the interface in each of these models and the results of experiments 3 and 4 are summarized in the Table 4. More literature values are available for these two experiments as it is apparent in this table. More diffusivity predictions are available at experiment 3 operating conditions since Upreti et al.'s results at these conditions have been used by others. Experiment 4 has been compared only with Upreti et al.'s results.

A specific point about these two experiments is that more fluctuations are observed in the trend of gas withdrawal from the supply cell. Referring back to eq 6, it is noted that this model works better when there is no gas accumulation in the gas cap by change in pressure. This is only true when a precise amount of needed gas (equivalent to gas-bitumen solubility demand) is injected during the diffusion process. Using the on-off operation between the supply and the diffusion cells for providing gas demand needs more care in the case of bitumen, because the rate of dissolution of CO₂ is about an order of magnitude slower than the rates in experiments 1 and 2. In the Error Analysis and Investigation of the Effect of Assumptions on the Final Solution section, the average pressure fluctuation in the diffusion cell is reported.

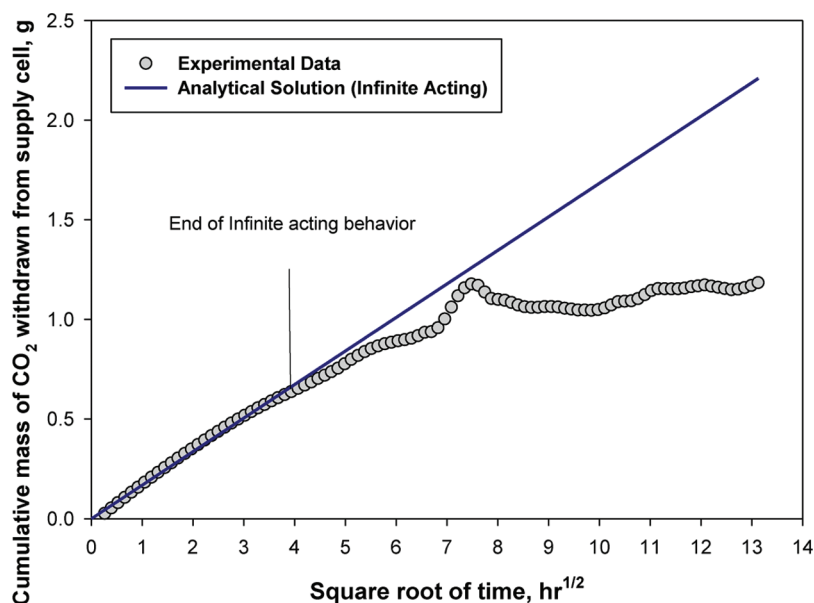


Figure 7. Cumulative mass of CO₂ withdrawn from the supply cell vs infinite acting analytical-model plot for $D = 5.00 \times 10^{-6} \text{ cm}^2/\text{s}$ and $C_g^* = 0.03414 \text{ g/cm}^3$; system of CO₂ and Athabasca bitumen at $P = 3239.6 \text{ kPa}$ and $T = 75^\circ\text{C}$.

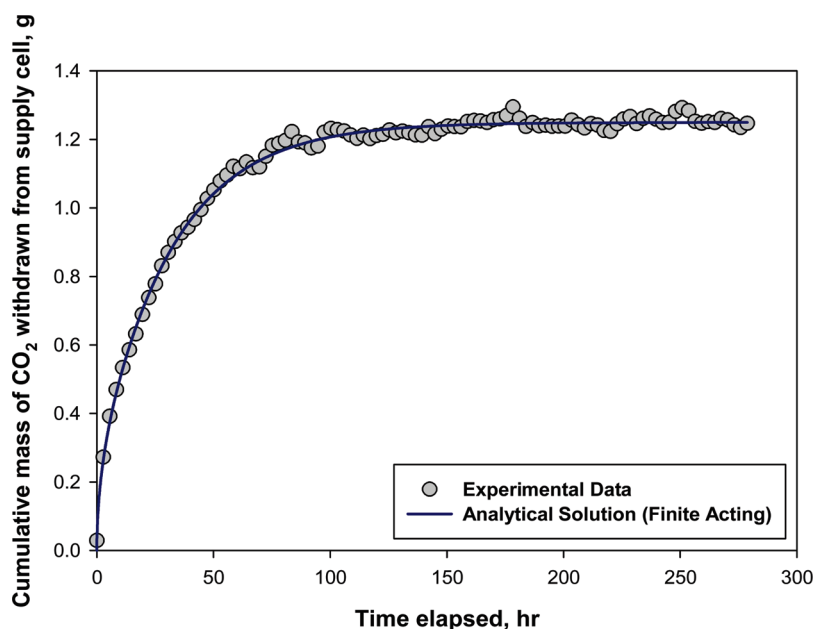


Figure 8. Cumulative mass of CO₂ withdrawn from the supply cell vs the finite acting analytical-model plot for $D = 3.60 \times 10^{-6} \text{ cm}^2/\text{s}$ and $C_g^* = 0.03934 \text{ g/cm}^3$; system of CO₂ and Athabasca bitumen at $P = 3804.8 \text{ kPa}$ and $T = 50^\circ\text{C}$.

Occasionally the pressure change in the diffusion cell becomes relatively large, by apparent malfunction of the control system. One of these malfunctions of the control system happened in experiment 3 as it is seen in Figure 6, however; we believe that this artifact has not affected the prediction of the diffusion coefficient and saturation concentration. In experiment 4, we have had a better control over the rate of addition of gas to the diffusion cell.

Figure 6 displays plots of the cumulative mass withdrawn from the supply cell to be dissolved in bitumen versus the model prediction. Although there is a drastic fluctuation around the 55th hour which surprisingly is followed by a decrease in the amount of gas which has left the supply cell, the part of information which are useful for us have remained

untouched and give us a decent overall prediction. Normally, we expect to predict the diffusion coefficient from an early time of the experiment and the saturation concentration from the late time. Figures 6 and 7 show how well the values of $D = 5.00 \times 10^{-6} \text{ cm}^2/\text{s}$ and $C_g^* = 0.03414 \text{ g/cm}^3$ match the early time (before 16th hour) and late time (after 120th hour) of the experiment. From Table 4, it is evident that the diffusion coefficient that was obtained for the third experiment using the minimization technique is close to the diffusivity values of Sheikha et al.¹ and Rasmussen et al.¹⁴ There is also a close agreement between the solubility value that we determined and the one that Rasmussen et al.¹⁴ reported for this experiment from the conventional pressure decay method. However, both our diffusivity and saturation

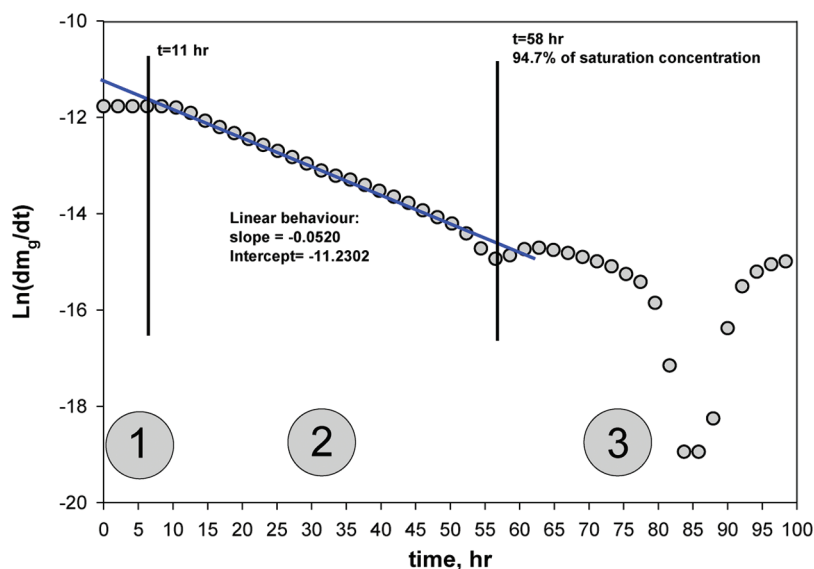


Figure 9. Determination of the diffusivity and saturation concentrations from the graphical method for experiment 1. The experimental results are divided into three regions based on this evaluation.

Table 5. Timing of Each of Three Sections in All Four Experiments from the Graphical Method

experiment	end of theoretical infinite acting period $t_{D1} \approx 0.1$, h	start of linear behavior, h	theoretical end of diffusion process time $t_{D1} \approx 1$, h	end of linear behavior, h	solubility at the beginning of scattered section (%)
1	5.14	11	51.44	58	94.7
2	5.78	14	57.87	140	99
3	6.00	7	60.05	36	78
4	7.72	8	77.16	69.7	89

concentration values are larger than the values of Upreti et al.¹⁰ As it was explained before, they had developed a numerical optimization technique to match the pressure decay such that a concentration-dependent diffusion coefficient had been determined. Nevertheless, what was reported in their 2002 paper¹⁰ for diffusivity was a set of averaged constant diffusion coefficients which is compared with our values here. The saturation concentrations reported in Table 4 for Upreti's work were estimated by extrapolation of their predicted instantaneous interface concentration to infinite time. Finally, experiment 3's pressure was selected to be equal to Upreti et al.'s saturation pressure (not their starting pressure).

Figure 8 illustrates the result of cumulative gas withdrawn from the gas supply cell versus the analytical model plot for $D = 3.60 \times 10^{-6} \text{ cm}^2/\text{s}$ and $C_g^* = 0.03934 \text{ g/cm}^3$. As can be seen, a decent match was obtained. Some small fluctuations are seen around 70–80 h, which is due to the fact that solution has reached to about 90% of its solubility and the rate of dissolution is lowered drastically, which makes our controlling system's job more difficult. As it is seen in Table 4, there are only Upreti et al.'s predicted values for comparison with our results. Again like the previous prediction values, our diffusivity and saturation concentration are close to theirs but somewhat larger. One more time it should be noted that Upreti et al.'s diffusivity value reported in this table is an average value of a concentration dependent diffusivity measurement.

Estimation of Diffusivity and Solubility Using the Graphical Method. On the basis of this method, the two unknowns are determined from the intercept and slope of $\ln(dm_g/dt)$ versus time plot. In Figure 9, a graph of these parameters has been plotted for the first experiment, and its intercept and slope

values are reported in the figure. As it is shown in this figure, this evaluation divides the experimental results into three regions. In the first region, a flat line is seen which is basically obtained as a result of numerical differentiation at the beginning of data points where possibly repeated data are used to calculate the derivative at one point. It was obtained that data portion of the first region belongs to the infinite acting part of diffusion process when the gas has not seen the effect of cell end. In Table 5, the equivalent time of diffusion dimensionless time 0.1 ($t_{D1} = Dt/h^2 \approx 0.1$) is calculated using the diffusion coefficients from the minimization technique as an indication of when theoretically the diffusion will reach to the end of the cell. As it is seen from the linear behavior start time, this region starts after $t_{D1} \approx 0.1$, which proves that the region of linear behavior (second region) starts after reaching the end of the cell.

With the data of region 1 put aside, the linear section is the section that has started after about $t_{D1} \approx 0.1$ and lasts up to approximately the 90% solubility amount. Thus, the period giving us this linear behavior is not only the early time period but it extends to late time. The reason for this is that the finite acting model solution which is valid for the entire course of the experiment (although only one eigenvalue is considered) is used for derivation of this method. The fact that this line belongs to a wide time range is the key for enabling us to find both unknowns from the same line. The period in which experimental data behave linearly is specifically illustrated in Figure 9 for the first experiment and is reported for other experiments in Table 5. The start of the third region is theoretically very close to the time equivalent of $t_{D1} \approx 1$, which conceptually means that the diffusion process has reached close to its completion. In Table 5, this time is reported

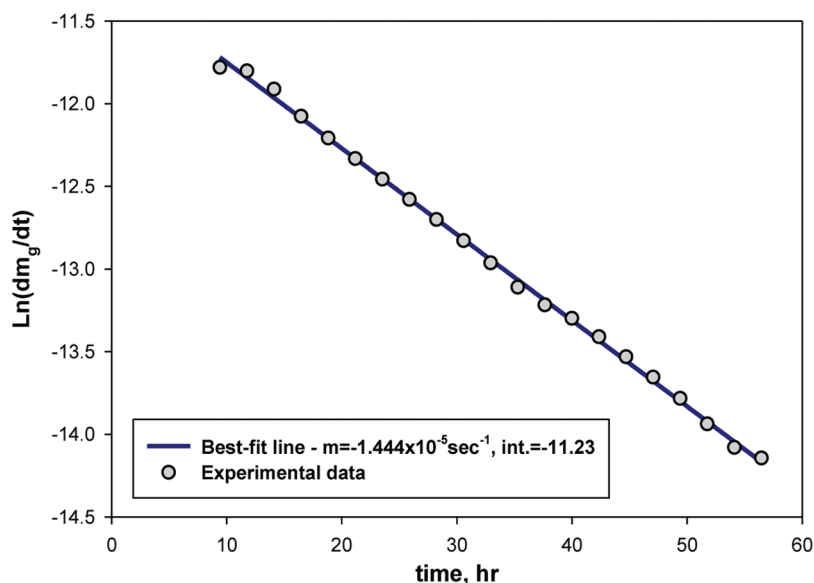


Figure 10. Linear regression of the 2nd region: experiment 1.

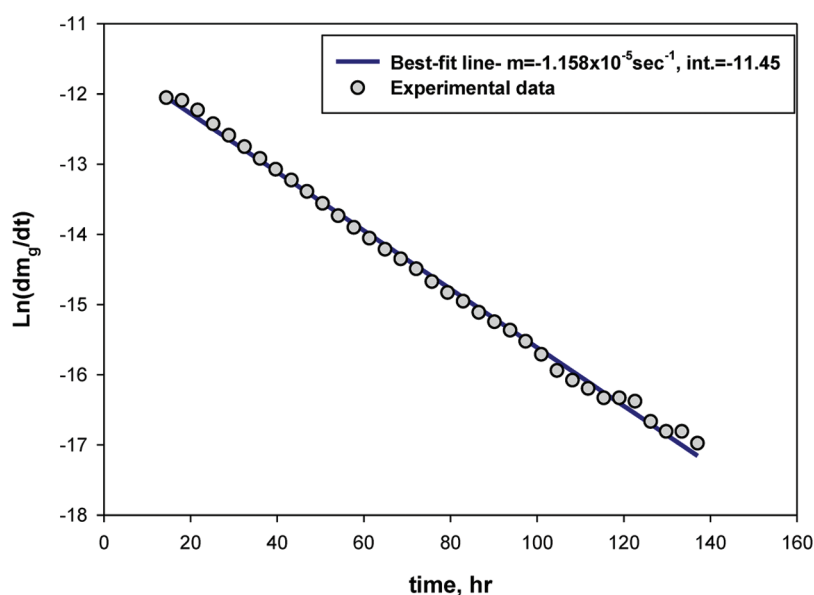


Figure 11. Linear regression of second region: experiment 2.

along with the time when we ended our evaluation of the second region. In the second region, the slope of the straight line gives us the diffusion coefficient and its intercept helps us find the solubility value. In Figures 10, 11, 12, and 13, the linear plots of each experiment are presented for the second region and the predicted diffusivity and saturation concentration results from the graphical method are all reported in Table 6. The regression R -squared values reported in this table show how well a linear pattern predicts the experimental data of the second region.

The saturation concentration and diffusion coefficients determined by the minimization technique are also reported in Table 6. Both values for experiment 1 determined by the graphical method are larger than the values determined with the minimization technique. However, values for the other experiments are in close agreement.

Comparison between the Two Methods. A comparison between these two methods shows that the graphical method is

definitely a simpler approach. It does not need any algorithm or computer code and provides both parameters with good precision. Only a portion of data is enough in this method to predict both unknowns as it is seen in Figures 10–13. In the minimization technique, we need to have good initial guesses for the two unknowns to find their values and there remains the question of the uniqueness of the solution since the minimum reached could be a local one. However, in the graphical method, the concern of uniqueness is not an issue. As long as the slope and intercept of the linear regressions are discernible, the diffusion coefficient and saturation concentration are obtainable.

Generally, a method which can determine the diffusion coefficient in a shorter run time is always desirable. With a single value concentration assigned at the interface, the determination of the both unknowns can be done in a shorter time and it is not necessary to have separately determined value of the saturation concentration. As it is indicated in Table 5, there is no need to wait for any part of region 3, and both unknowns

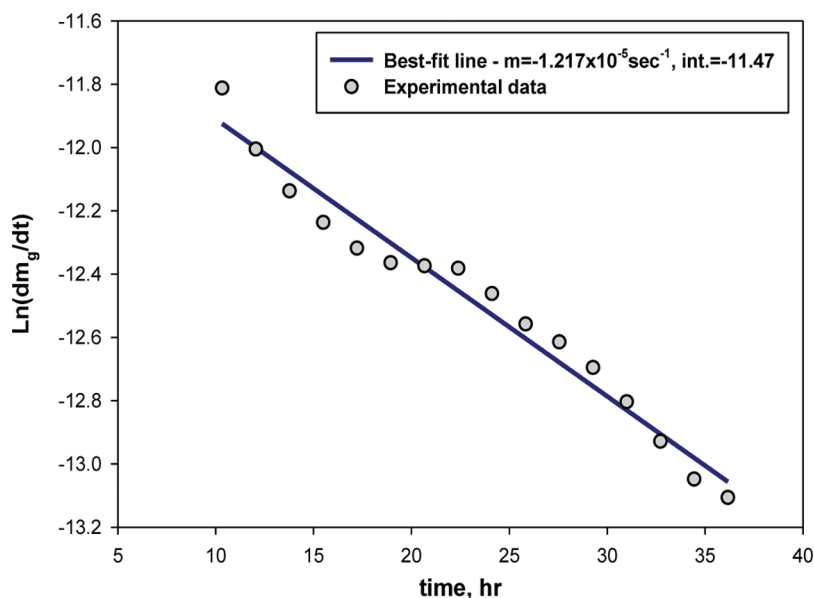


Figure 12. Linear regression of second region: experiment 3.

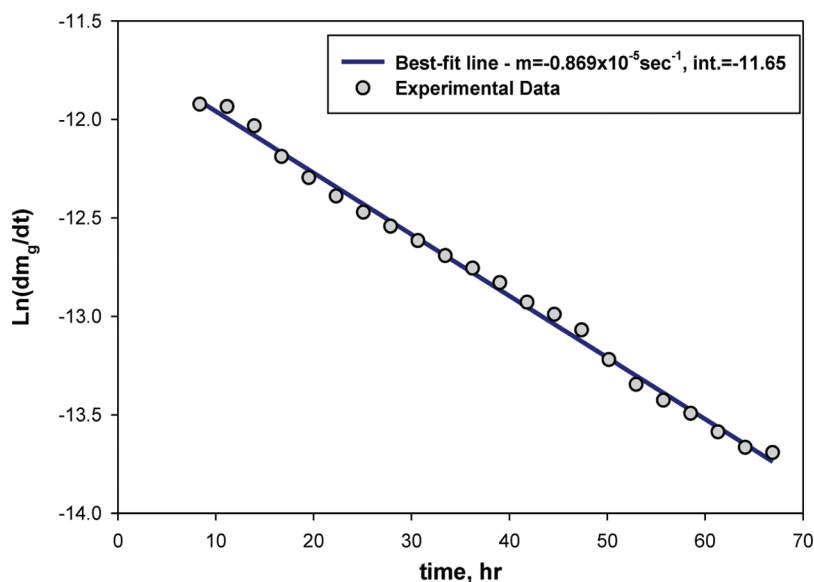


Figure 13. Linear regression of second regions: experiment 4.

Table 6. Results of the Graphical Method and Its Comparison with the Minimization Approach Results

experimental gas–liquid system		minimization technique		graphical technique		
		D (cm ² /s)	C_g^* (g/cm ³)	D (cm ² /s)	C_g^* (g/cm ³)	R^2
experiment 1	CH ₄ in dodecane	4.86×10^{-5}	0.011 03	5.28×10^{-5}	0.011 93	0.9987
experiment 2	CH ₄ in dodecane	4.32×10^{-5}	0.011 68	4.22×10^{-5}	0.011 71	0.9971
experiment 3	CO ₂ in bitumen	5.00×10^{-6}	0.034 14	5.25×10^{-6}	0.033 87	0.9681
experiment 4	CO ₂ in bitumen	3.60×10^{-6}	0.039 34	3.55×10^{-6}	0.039 11	0.9959

are predictable from the earlier data. For the minimization method, we need to run the experiment only for several hours beyond the time when the concentration distribution reaches the end of the cell. The finite acting model is able to distinguish and predict both values from such data. This justification works for the graphical method also. If we have a portion of data after $t_{D1} \approx 0.1$ and the slope and intercept are clearly discernible, then there is no need to run the experiment for longer periods.

Table 7. Average Value of Pressure Fluctuation in Diffusion Cell in Each Experiment

experimental runs		average pressure fluctuation, kPa	relative error % $\Delta P_{diff}/P_{diff}$
experiment 1	CH ₄ in dodecane	6.99	0.20
experiment 2	CH ₄ in dodecane	2.51	0.07
experiment 3	CO ₂ in bitumen	6.95	0.21
experiment 4	CO ₂ in bitumen	7.44	0.19

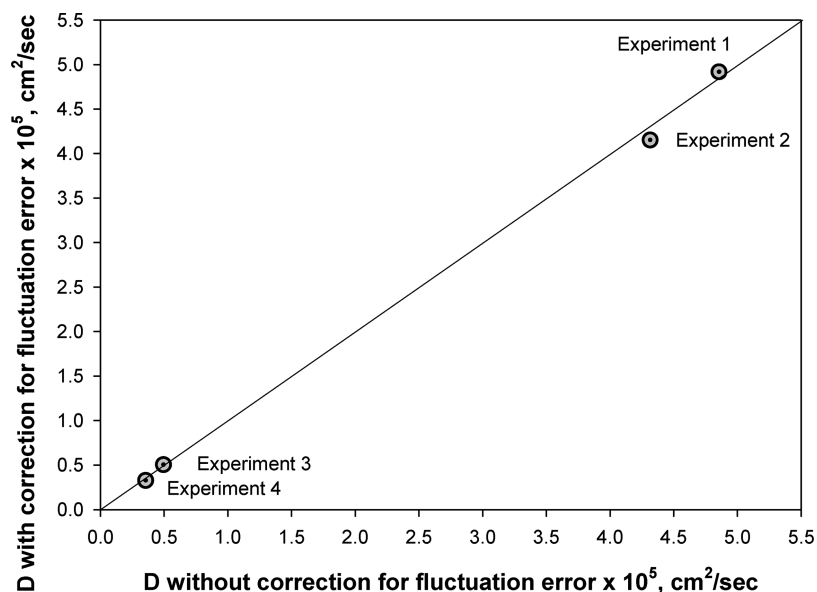


Figure 14. Effect of correcting for pressure fluctuation error in the gas cap on the predicted diffusivity value.

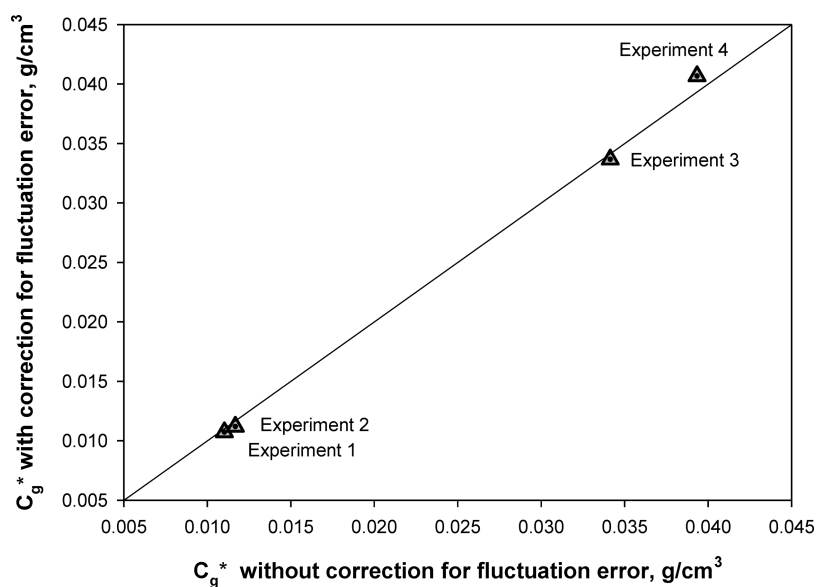


Figure 15. Effect of correcting for pressure fluctuation error in the gas cap on the predicted saturation concentration.

Error Analysis and Investigation of the Effect of Assumptions on the Final Solution. As the first step in error analysis, the uncertainty in the data that are used to calculate mass of dissolved gas is calculated. The random error in reading the temperature in both the supply and diffusion cells is 0.01 °C. The random errors in the supply cell and diffusion cell pressure measurements are 0.007 and 0.002 kPa, respectively. On the basis of these values, the error bar for each point measurement of the amount of gas dissolved would be in the range of ± 0.016 g.

Error Due to Pressure Fluctuation in the Diffusion Cell. As it was explained in the Experimental Equipment and Measurements section, the connection between the gas in the supply cell and diffusion cell is established through two electronic valves. This connection is not continuous but intermittent, as dictated by the controller. This causes a small pressure buildup every time gas goes into the diffusion cell. The average amount of pressure fluctuation and the relative

Table 8. Density Change and Investigation of Density Induced Convection Possibility in Experiments 1 and 2

experiments	density of pure C_{12} at T_{exptl}^a (g/cm ³)	density of saturated C_{12} at T_{exptl} (g/cm ³)
experiment 1: CH ₄ in dodecane at 65 °C	0.7166	0.6036
experiment 2: CH ₄ in dodecane at 45 °C	0.7308	0.6114

^a Refer to ref 29.

error related to this fluctuation is reported in Table 7. In derivation of the model, this small pressure fluctuation was neglected by assuming that all the gas leaving the supply cell dissolves into the liquid. However, it is possible to correct for

(29) Yaws, C. L. *Yaws' Handbook of Thermodynamic and Physical Properties of Chemical Compounds*; Knovel: Norwich, NY, 2003.

(30) Upreti S. R. *Experimental Measurement of Gas Diffusivity in Bitumen: Results for CO₂, CH₄, C₂H₆, and N₂*; University of Calgary: Calgary, Canada, April 2000.

Table 9. Investigation of Swelling Factor Magnitude

experiment	initial liquid height cm	estimated liquid height increment at C_g^* , cm	relative error %	diffusion coefficient after swelling cm^2/s	saturation concentration after swelling g/cm^3
1 ^a	12.3	0.2	1.6	5.02×10^{-5}	0.010 85
3	1.055	0.040	3.79	5.38×10^{-6}	0.032 90
4	1.005	0.044	4.38	3.71×10^{-6}	0.038 59

^aFrom Jamialahmadi et al.'s work. Refer to ref 2, Figure 4a.

this error in the calculation of the amount of gas dissolved in the liquid by adding a correction term to eq 6 as in eq 23.

$$m_{\text{g-diss}}(t) = m_{\text{g-tr}}(t) - m_{\text{g-fluc}}(t) = \frac{Mw}{R} \left(V_{\text{SC}} \left(\frac{P_{\text{ini}}}{Z_{\text{ini}} T_{\text{ini}}} - \frac{P(t)}{Z(t) T(t)} \right)_{\text{SC}} - V_{\text{GC}}(t) \left(\frac{P_{\text{GC}}(t)}{Z(t) T_{\text{GC}}(t)} - \frac{P_{\text{diff}}}{Z_{\text{diff}} T_{\text{diff}}} \right) \right) \quad (23)$$

in which $m_{\text{g-tr}}(t)$ is the same as calculated from eq 6 but it is now corrected by subtracting the fluctuation term, i.e., $m_{\text{g-fluc}}(t)$. In this equation, $V_{\text{GC}}(t)$ is the volume of gas cap (which shrinks a bit due to the swelling of the solution), P_{diff} and T_{diff} are the target pressure and temperature at which we measure the diffusivity, and $P_{\text{GC}}(t)$ and $T_{\text{GC}}(t)$ are the actual gas cap pressure and temperature that are recorded every minute. On the basis of the corrected values of the amount of gas dissolved ($m_{\text{g-diss}}(t)$), the diffusion coefficient and saturation concentration were recalculated. However, the new values are very close to the previous values. The new values determined have been compared with the original uncorrected ones, and these comparisons are shown in Figures 14 and 15.

It is evident that the effect of correcting for this fluctuation is not very significant since the plotted points are all close to the equity line. The maximum diffusivity change is related to experiment 4, which is about 11%, and all the saturation concentration changes due to adding the fluctuation term are less than 4%.

Liquid Is Nonvolatile and Diffusion Is One Way. This assumption seems to be valid based on the information that was determined from two different sources. Experiments 1 and 2 were at the same conditions using the same components as in the experiments of Jamialahmadi et al.² They have reported that the composition of the gas phase was analyzed with a gas chromatograph (at the end of each experiment) to check the possibility of evaporation of the liquid phase, which was found to be negligible. In the same sense, Badamchizadeh et al.,²⁰ who used the same bitumen as what was used in experiments 3 and 4, have reported in their work that based on their compositional analysis, no gas or light components exist in this bitumen to show volatility during the diffusion process. Thus, we may conclude that the diffusion process has been in only one direction, from gas to liquid. Consequently, the assumption of having a one-way diffusion from gas to liquid is valid.

No Density Induced Convection Currents. The CMG Winprop module was used to predict the density of the methane–dodecane solution at the operating conditions of experiments 1 and 2. On the basis of this evaluation, the density of normal dodecane declines as in Table 8 and there will not be any increase in the density of solution to cause density induced convection currents. In regards to experiments 3 and 4 also, it should be mentioned that since the viscosity of bitumen is very high and the liquid column height is small,

the presence of density induced convection current can be neglected even if the solution of CO₂ and bitumen is marginally denser than the virgin bitumen.

Swelling Effect. Since our cell was a blind cell, the measurement of swelling was not possible by tracking the movement of the interface. Nonetheless, calculation of this interface movement is possible if we calculate the liquid volume change using the solubility amount and ideal mixing rule. For the first two experiments, the swelling data is available in Jamialahmadi et al.² from which when the relative error due to swelling was calculated for experiment 1; it was less than 2% and is considered negligible.

In experiments 3 and 4, provided that the mixture of CO₂ and Athabasca bitumen can be assumed to follow ideal mixing, the relative error due to neglecting the swelling is less than 4.5% as it is shown in Table 9. However, it is likely that the solution of CO₂ and bitumen does not obey ideal mixing and the volume of mixture is expected to be less than the summation of both species' volumes. A sensitivity analysis was done to find the boundary of diffusivity and saturation concentration with and without swelling. The predicted values of the two unknowns at the estimated maximum swelling bounds are reported in Table 9. On the basis of our sensitivity analysis, it turns out that for the same dissolution rate, once the oil swells, the diffusion coefficient increases and the saturation concentration decreases. This seems reasonable because in the case of having a larger liquid column, the diffusion coefficient should be larger to move the gas molecules in the oil faster to meet the same dissolution rate pattern. On the other hand, because the amount of gas dissolved remains the same but the volume changes, the saturation concentration term shrinks. The relative errors due to neglecting the swelling are 7.6% and 3.0% for diffusivity values and 3.6% and 1.9% for saturation concentration for experiments 3 and 4, respectively.

Conclusions

A fully automated constant-pressure gas diffusivity measurement technique has been developed which is suitable for diffusivity and solubility measurements at high pressures. The idea behind conventional pressure decay method is used here for calculation of dissolved gas amount while the pressure is kept constant at the liquid interface. The constant value for interfacial concentration allows determination of the gas saturation concentration (at a specific temperature and pressure) from the same experiment. A parameter estimation routine and a simple graphical technique were developed for analyzing the experimental data to simultaneously determine the diffusion coefficient and gas solubility. The diffusivity values determined by using this modified pressure decay technique are consistent with values reported by others.

Acknowledgment. We thank the Computer Modeling Group for providing us access to the CMG Winprop module. The first author acknowledges financial support and funding by NSERC and the Alberta Ingenuity Fund.

Nomenclature

C = concentration, g/cm³
 t = time elapsed, s
 z = vertical space coordinate, cm
 D = diffusion coefficient, cm²/s
 P = pressure, 1-kPa
 V = volume, cm³
 m = mass, g
 Z = gas compressibility
 h = quiescent liquid height, cm
 H = height of swelled liquid in each step, cm
 e = error
 S = summation of squared error between experimental and computed values
 f = an arbitrary function
 g = an arbitrary function
 J = Jacobian matrix
 M_w = molecular weight, g/g-mol

Symbols

∞ = infinity

Subscripts

g = gas
 ini = initial

SC = supply cell
 tr = transferred
 r = remained
 i = iteration parameter
 p = iteration parameter
 k = number of experimental recorded points
 eq = equilibrium
 D = diffusional term
 DI = dimensionless
 GC = gas cap
 $diss$ = dissolution
 $diff$ = diffusion
 $fluc$ = fluctuation

Superscripts

*, asterisk = saturation state

Abbreviations

BC = Boundary Condition
 CAT = computer assisted tomography
 CMG = Computer Modeling Group
 EOS = equation of state
 NI = National Instruments
 NMR = nuclear magnetic resonance
 PD = pressure decay
 PR = Peng–Robinson